The Influence of Metal Nanoparticle Size Distribution in Photoelectron Spectroscopy

L. Minati,*,† G. Speranza,† L. Calliari,† V. Micheli,† A. Baranov,‡ and S. Fanchenko§

FBK, Sommarive Street 18, 38050 Povo-Trento, Italy, MATI-RGTU, Moscow, Russia, and RRC Kurchatov Institute, Moscow, Russia

Received: March 10, 2008; Revised Manuscript Received: June 19, 2008

We present an innovative approach to characterize small metal nanoclusters embedded in an amorphous carbon matrix. A simple mathematical relation linking binding energy shifts to the mean nanoparticle (NP) dimensions allows determination of the distribution of NP sizes by fitting the Au 4f X-ray photoemission spectrum. The NP size distributions obtained using our method are compared with those obtained from X-ray diffraction spectra.

Introduction

The unique properties of small metal nanoparticles have been well-known for some years. They are extensively used in catalysis,[1] optics,[2] biosensing,[3] and so forth. Because of this large field of use, a great number of synthesis procedures have been developed in the last decades. The ability to control the dimensions and size distribution of nanoclusters is of paramount importance in material science. In a previous paper, we proposed magnetron sputtering (MS) as a fast, efficient, and low-cost process for the synthesis of carbon−platinum and carbon−gold thin films, which can be successfully used as electrodes within electrochemical gas sensors.[4] MS provides a single-stage process, without requirement of any kind of solvent. Films of about 50 nm thickness are rapidly produced in about 20 min of processing and by consuming a considerably low amount of precious metal. From the analytical point of view, X-ray photoelectron spectroscopy (XPS) is one of the most effective techniques for the study of metal nanoclusters because it can provide both chemical and structural information. In this respect, for small metal nanoparticles (with diameters lower than 5 nm), an estimation of the mean dimension is gained by analyzing the core line binding energy (BE) shift and the valence band narrowing with respect to the bulk counterpart.[5] The advantage of this approach is related to the high sensitivity of XPS to very small clusters. Imaging techniques, like transmission electron microscopy (TEM), cannot unambiguously resolve particles smaller than 1 nm. In contrast, XPS is sensitive to the quantum confinement effect, which increases when the NP size decreases. Nonetheless, the effect of subnanometer dimensions on the properties of nanoparticles (NPs) is, nowadays, not completely understood. For this reason, sophisticated analysis tools to determine the precise size distribution of nanoparticles are even more crucial.

The ability to determine the nanoparticle size distribution is of paramount importance in particular for catalysis, where cluster dimensions are normally correlated to the catalyst efficiency. This is why the presence of subnanometer NPs may heavily affect the system reactivity.

As an example, we can consider the case of gold NPs supported on TiO_2. This catalyst shows an extraordinary catalytic activity even at low temperature in the carbon monoxide oxidation reaction.[6] The turnover frequency of this reaction strongly depends on the average particle size, with higher catalytic activity for particle size of about 2−3 nm.[7] However Anderson et al.[8] pointed out that also subnanometer Au_n ($n = 3-7$) clusters on TiO_2 possess catalytic activity toward CO oxidation. The enhanced catalytic activity is linked to the rearrangement of electrons of gold atoms occurring when the long-order distribution of the electronic charge in bulk metals approaches the nanometric dimensions in clusters. This change in the electronic configuration influences also the X-ray photoemission process.

Shifts to higher binding energy (BE) of the core line obtained from metal nanoclusters, with dimensions lower than 5 nm, with respect to the bulk value are widely reported in the literature.[9,10] Some authors associate these shifts with an initial state effect produced by a modification of the repulsive interaction between core levels and valence bands (sp−d rehybridization).[10] Others explain it as a final state effect due to the inability of the system to shield the core hole created in the photoemission process (extra atomic relaxation). This leads to a kinetic energy loss as a consequence of a transitory charging of the nanoparticle during the photoionization process.[11] Although both initial and final state effects contribute to modify XP spectra, the exact description of the origin of BE shifts is out of the topic of this paper.

Here, we present an XPS study of a-C/Au samples produced by magnetron sputtering (MS) deposition, and we discuss the use of the Au 4f core lines to determine the mean clusters dimensions and distribution.

Experimental Section

a-C/Au nanocomposite films were deposited on silicon wafers by magnetron cosputtering of C and Au in Ar at a temperature of 20−50 °C. The input magnetron power was 140 W. The silicon wafer was mounted on a substrate holder rotating at a speed of 3.14 rpm. The growth rate was about 2 nm/min. The working gas pressure in the vacuum chamber was 1.5×10^{-3} Torr. Metal gold plates were placed on the graphite target with different Au-to-graphite surface ratios in order to obtain variable concentrations of Au in the deposited films. Two different a-C/Au samples, referred to as CAu 1 and CAu 2, were produced. Their Au content, as revealed by XPS, was 8 and 12.5 atom %, respectively. The thickness of the nanocomposite layers, measured by X-ray reflectivity, was about 40 nm. The samples were

---

* To whom correspondence should be addressed. E-mail: luminati@fbk.eu.
† FBK.
‡ MATI-RGTU.
§ RRC Kurchatov Institute.

10.1021/jp804169q CCC: $40.75

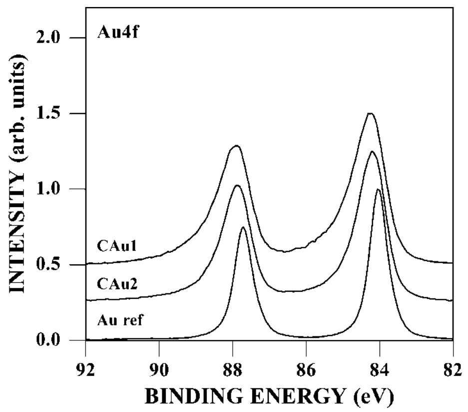

Figure 1. Au 4f spectra of the bulk Au sample as well as the CAu 2 and CAu 1 samples after Shirley background subtraction. The intensity of the lines is normalized to a common value.

transferred in containers under nitrogen atmosphere immediately after the deposition until the introduction in the XPS instrument to minimize the contamination.

XPS measurements were carried out using an ESCA200 instrument (Scienta-Gammadata ESCA 200 Uppsala Sweden) equipped with a monochromatic Al Kα ($h\nu = 1486.5$ eV) X-ray source. Wide scans were acquired in the BE energy range of 1200−0 eV using a 500 eV pass energy, while high-resolution core line spectra were acquired at 150 eV analyzer pass energy and with an energy step of 0.05 eV. Because the samples are conductive, they did not require charge compensation, leading to an energy resolution of 0.3 eV. Au 4f core lines were normalized to a common intensity after Shirley background subtraction. The C 1s binding energy is 284.6 eV, corresponding to carbon having graphitic nature. XP spectra were acquired also on a pure (99.99%) sputter-cleaned gold sample (referred to as Au ref), which was taken as a reference for data manipulation. The algorithm for the calculation of the size distribution was implemented in the GNU-Octave framework.

XRD patterns were obtained with an APD 2000 X-ray diffractometer with the Cu Kα radiation source operated at 40 keV with a 2θ step of 0.05° and acquisition time of 5 s. XRD results were analyzed by modeling an analytical profile shape function. A Pearson VII function was used for profile fitting after proper background subtraction and Rachinger alpha-2 correction. The distance between two peaks, assigned to the 111 and 200 reflections, was kept at $2\theta = 6.2°$, as that for bulk gold, stabilizing the fit. The instrumental-dependent broadening was removed by Stokes deconvolution. The size distribution was calculated by Fourier analysis following the Warren−Averbach method. For spherical particles of diameter D, the size in the direction normal to the sample surface should be taken as the averaged height of the sphere, $2D/3$. The Fourier coefficients are plotted versus the domain size. The second derivative of Fourier coefficients with the domain size gives the size distribution.

Result and Discussion

Xps Analysis. In Figure 1, we report the Au 4f core line obtained from the gold reference and from CAu 1 and CAu 2 samples. There are marked as differences in the Au 4f doublets of the three samples. In particular, the peaks of the two a-C/Au samples are characterized by a high full width at half-maximum (fwhm) and a pronounced asymmetry. Considering the NP reactivity, modification of the Au 4f core line features could be induced by a chemical bond between gold and other elements. This can be excluded for our samples. The wide scan revealed the presence, besides carbon and gold, of oxygen, which amounts to ∼3−4 atom % in both samples. An accurate analysis of the O 1s and C 1s core line shows that the oxygen atoms are bonded only to the carbon network. This is also confirmed by the absence of any spectral component in the Au 4f core line at the energy of Au_2O_3, around 86 eV.[12] This is in agreement with the literature where the oxidation of gold was obtained only under special conditions, like high temperature or with treatments with reactive oxygen plasmas. Finally, these results are also in agreement with other works devoted to the study of possible chemical reactions occurring in a-C/H/Au samples exposed to air. After keeping a-C:H/Au nanocomposites for 20 h in air, Videnovich et al.[13] revealed only a change in the atomic abundances due to contaminants, while the Au 4f line shape was identical to the original. All of these findings point to the conclusion that the spectral changes of the Au 4f lines with respect to Au ref, as shown in Figure 1, are produced by a distribution of gold nanoparticles. The position of the metal cluster core lines depends on various factors like the nature of the metal and that of the support as well as the shape and dimensions of the nanoparticle.[14] Supported metal nanoparticles can be considered as small spherical capacitors, which are charged by photoelectron emission. From this viewpoint, the BE shift follows the $e^2/\varepsilon_r\varepsilon_0 D$ law, where D is the nanoparticle diameter and ε_r is the dielectric constant of the surrounding medium.[15] However, this is a too raw simplification because it does not account for the initial state effect, leading to a bad portrayal of the experimental data. Moreover, for clusters with $D > 5$ nm, the assumption of a spherical condenser breaks down. The core hole will relax sufficiently fast, the final state effect will disappear, and the model of a charged condenser will fail.[5] We solved this problem by collecting a set of BE values corresponding to populations of monodispersed NPs with known dimensions from the literature.[16–18] This is a crucial point since it determines the accuracy in estimating the BE as a function of the NP size. The set of data was fitted using the following function:

$$\mathrm{BE}(D) = \mathrm{BE_b} + k_1 \cdot e^{k_2 \cdot D^{k_3}} \qquad (1)$$

where D represents the NP diameter and k_1, k_2, and k_3 are fitting parameters. We note that eq 1 was not derived on the basis of physical assumptions but was selected among those that better represent the experimental data. The quality of the results is shown in Figure 2 where the BE(D) curve obtained from eq 1

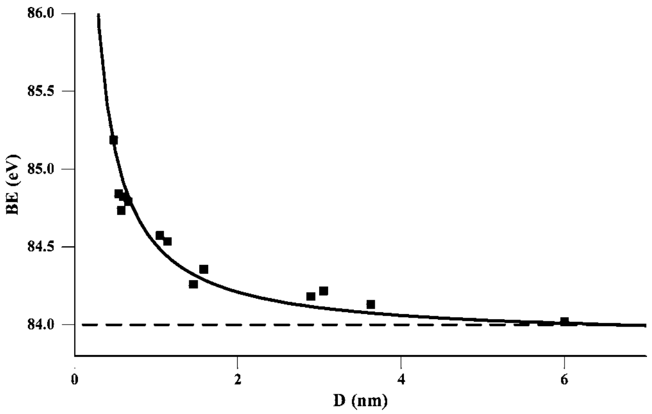

Figure 2. Plot of the Au 4f BE as a function the nanoparticles diameter. Full square: gold clusters deposited on a substrate obtained from refs 13–15. The continuous line represents the fit function described by eq 1. The dashed line represents the BE value of the bulk gold sample.

is plotted together with the set of literature data corresponding to populations of monodispersed NPs with known dimensions.[13–15] We observe that for $D \geq$ 6nm, where the effects of confinement disappear, BE(D) correctly flattens around the bulk Au 4f energy position (BE_b), allowing us to use this function to estimate the NP distribution.

These results are obtained in the hypothesis that nanoparticles have spherical shape and are fully embedded in the carbon matrix. It is known that gold possesses a higher surface free energy with respect to carbon. If the sum of the free energy of gold and that of the gold−carbon interfaces is bigger than that of carbon, the system is expected to grow according to the Volmer−Weber mode.[19] This leads to the formation of 3D single-domain gold particles. Moreover, the low solubility of gold in carbon avoids the formation of a gold−carbon alloy and promotes the precipitation of Au NPs during deposition.[20] Finally, since carbon and gold are cosputtered, the NP growth is controlled by the continuous deposition of carbon, which forms the supporting matrix and limits the NP dimensions at the same time. Under these conditions, the Ostwald ripening effect is low, and we will obtain rather small spherical-shaped nanoparticles with a certain spread of dimensions.

The second assumption regards the position of the gold nanoparticles inside of the carbon matrix. The relative position of the gold nanoparticles in the matrix can affect heavily the sample properties but has little influence on the photoelectron spectra. First of all, we must consider that the nanoparticles could be fully or partially embedded. This can easily be determined by angle-resolved XP measurements. Our results (not reported here) point out that, at grazing emission, the Au/C intensity ratio decreases with respect to normal emission. This result corresponds to fully embedded NPs or NPs covered by a thin layer of carbon, in agreement with the conclusions of Videnovich.[15] Further support to this statement comes from the great time stability of the a-C/Au samples. Because of its weak interaction with carbon, gold is known to have great mobility on the surface of HOPG or a-C. Au 4f core and valence spectra of sample CAu 1 acquired after 1 year can be perfectly superimposed on the original ones. This can be explained by steric stabilization due to the carbon, giving credit to the assumption of fully embedded NPs. The BE shift for clusters in different positions with respect to the sample surface depends on the dielectric constant of the surrounding media. The relation between cluster size and core level shift is described in detail in some of the references cited, such as Wertheim et al., Boyen et al., or Thune et al. The photohole created during the photoemission process has to be described as a dynamic process.[21] During the travel of the electrons from the clusters to the sample surface, the NP remains charged for some time. If this time is long enough, the charged NP directly influences the kinetic energy of the photoemitted electron and, at the same time, the surrounding medium that, in its turn, shields the photohole. Gold nanoparticles deposited by MS are expected to grow with a certain size distribution that depends primarily on the amount of gold in the film. The Au content can be controlled by varying the gold/graphite relative area exposed to erosion while keeping the other experimental parameters constant. Such a kind of gold NP population can be described by a log-normal distribution of sizes, which was already used to successfully describe TEM results.[22] In order to compare our result with those obtained by other techniques, we have modified the numerical-weighted log-normal distribution. In the case of XPS, the spectral intensity is proportional to the number of irradiated atoms. To account for this effect, we introduce a function $\xi(D)$ that describes the instrumental response as a function of the nanoparticle dimension. To work out an expression for $\xi(D)$, we assume gold nanoparticles with spherical geometry placed just beneath, and in touch with, the sample surface. The contribution of a single NP section parallel to the sample surface is proportional to the section volume. In a polar coordinate system, with the origin at the center of the NP, the azimuthal plane parallel to the sample surface, and the polar angle θ, the contribution of a NP section is proportional to the section volume weighted by an exponential decay involving the electron inelastic mean free path (IMFP) λ.[23] Since we have checked that accounting for differences in the IMFP of the matrix and of the metal particle changes the function $\xi(D)$ by just a few percent, we have considered only the Au IMFP, λ=1.7 nm. The resulting expression for $\xi(D)$ for normal takeoff angle is

$$\xi(D) = K \cdot \int_0^{\pi} \pi\left(\frac{D}{2}\sin\theta\right)^3 e^{-\frac{D}{2}(1-\cos\theta)/\lambda} d\theta \tag{2}$$

Constant K accounts for all parameters affecting the XPS intensity, such as the photoelectron cross section, the detector efficiency, and so forth. Of these parameters, some depend only on the system under study, like the Au 4f photoemission cross section, while others, like the detector efficiency and the X-ray source emission efficiency, depend on the instrument.

Assuming a log-normal distribution of NPs, we may write the XP intensity as $I(D,\mu,\sigma)$

$$I(D,\mu,\sigma) = \frac{e^{-(\ln(D)-\mu)^2/(2\sigma^2)}}{\sigma D\sqrt{2\pi}} * \xi(D) \tag{3}$$

where μ and σ are the distribution mean and variance, respectively. Equation 1 can now be used to obtain D as a function of the BE, so that the signal intensity I can be given as a function of the BE. $I(\mathrm{BE},\mu,\sigma)$ shows a great asymmetry due to the spread of cluster dimensions. To describe the experimental data, we must account for spectral broadening due to the natural line width of the core line and to the instrumental resolution. To this end, $I(\mathrm{BE},\mu,\sigma)$ is convoluted with a Voigt function $V(\mathrm{BE},m,W,M,\alpha)$, where m represents the peak position, W the peak width, M the Lorentzian−Gaussian fraction, and α the singularity index. This line shape was selected because it correctly reproduces the Au 4f core line of bulk gold. The resulting function

$$g(\mathrm{BE},\mu,\sigma) = I(\mathrm{BE},\mu,\sigma) \otimes V(\mathrm{BE},m,W,M,\alpha) \tag{4}$$

was used to fit the experimental spectra. Here, μ and σ were free parameters in the fitting procedure. At variance with many metals, the bulk Au 4f spectrum shows a very low asymmetry α. Since the asymmetry depends on both the density of states at the Fermi level and the core hole potential screening,[24] which decrease with the scaling of the particle size, the α value was initially set to zero in the iterative process.

On the other hand, the reduction of metal particles to nanometric size could induce changes in the core line width and shape caused by metal-to-nonmetal transition. This effect was extensively studied in the past by some authors. Due to the overlap of different effects (initial, final, nanoparticle reshaping, interaction with the supporting substrate), a clear identification of the effect of the core hole lifetime on the width of the core line is still not totally discerned. Recently, Boyen et al. reported on the metallic nature of Au_{55} clusters (D = 1.4 nm), while nonmetallic properties were shown for Au_{33} (D = 1.03 nm).[25] Transition from metal to nonmetal induces an increase in the core line width due to the increase of the

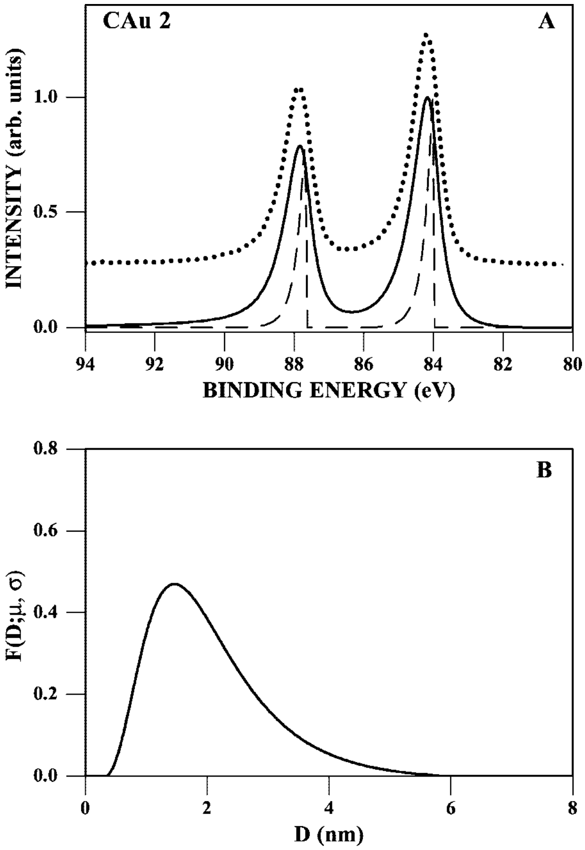

Figure 3. (A) Fit of the Au 4f core line of sample CAu 2 after background subtraction. Dashed line: representation of the $I(\mathrm{BE},\mu,\sigma)$ function. Solid line: convolution with Voigt broadening eq 4. Dotted line: Au 4f of the CAu 2 sample. (B) Size distribution function obtained from the iterative process.

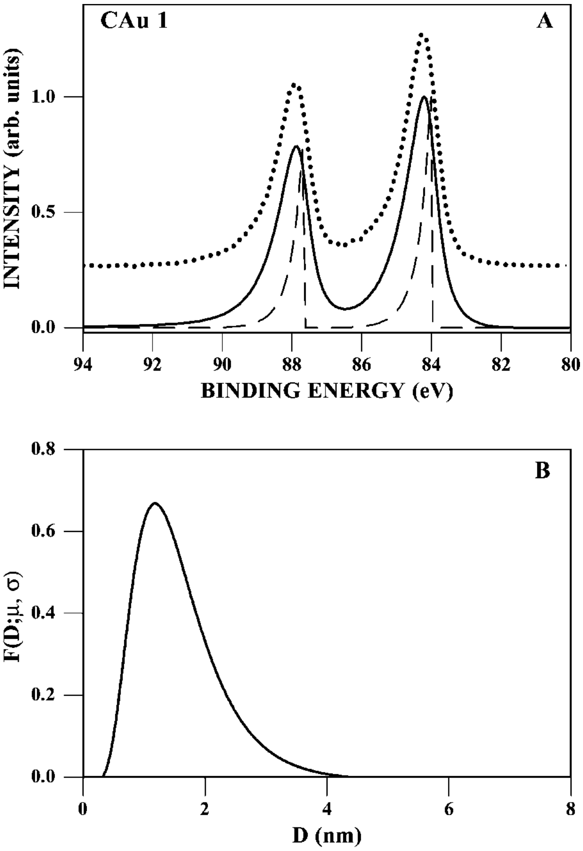

Figure 4. (A) Fit of the Au 4f core line of sample CAu 1 after background subtraction. Dashed line: representation of the $I(\mathrm{BE},\mu,\sigma)$ function. Solid line: convolution with Voigt broadening eq 4. Dotted line: Au 4f of the CAu 1 sample. (B) Size distribution function obtained from the iterative process.

photohole lifetime. Dicenzo et al.[17] investigated the Au 4f core line of size-selected gold nanoclusters deposited on amorphous carbon. These core lines showed an increased width with respect to the bulk Au 4f core lines. The line width remains quite constant from Au_{33} to Au_7 clusters, while for Au_5, a shoulder at high BE is observed, which the authors associate with small atom aggregates derived from the fragmentation of the clusters. In this respect, we note that it is very difficult to separate the line shape change due to the core hole lifetime from line broadening due to the cluster size distribution. In particular, because of the quasi-hyperbolic dependence of the BE with respect to D (see Figure 1), a small change in the dimension causes a big change in the BE. As a consequence, the presence of a NP size distribution leads to significant broadening of the core line. Another modification of the line shape arises from the interaction between nanoparticle surface atoms and the environment.[26] This effect is expected to increase due to the increasing surface to volume ratio as the NP size decreases. However, for a weak interaction between the metal and the support, as in our case, the effect can be neglected.

Results of the calculation for the two a-C/Au samples are shown in Figures 3A and 4A. The dotted line is the experimental spectrum, the dashed line represents the calculated photoelectron yield $I(\mathrm{BE},\mu,\sigma)$, while the solid line is the Voigt broadened curve, $g(\mathrm{BE},\mu,\sigma)$. All spectra are normalized to a common height of the Au $4f_{7/2}$ peak. We see that function $g(\mathrm{BE},\mu,\sigma)$ reproduces the experimental spectrum well. Figures 3B and 4B show the log-normal distribution for sample CAu 1 and CAu 2, respectively. Both distributions are peaked at a NP size < 2 nm. These distributions account for the pronounced asymmetry of the Au 4f core lines of samples CAu 1 and CAu 2. They reveal, in fact, that a high number of clusters of small dimensions are present in these samples. The smaller the cluster size, the lower its photoelectron yield, but the higher the BE shift of its spectral contribution with respect to the bulk Au 4f spectrum. The log-normal distributions indicate that there is, on the contrary, a small number of big (>4 nm) NPs whose signal intensity is, however, compensated by the high number of atoms composing the NPs. The BE shift of their spectral contribution with respect to bulk gold goes to zero with increasing NP dimension. Looking at the two core lines, it is clear why we have chosen size-selected clusters for the calibration curve in Figure 2. It is evident that errors can be introduced by using only the position of the curve maximum without analyzing the entire line shape. As an example, the sample CAu 2 is shifted by 0.13 eV with respect to the position of bulk Au 4f. Using the calibration curve of Figure 2, we would estimate a mean particle size of around 3.8 nm. On the contrary, by considering the whole size distribution, as obtained from the Au 4f line shape analysis, we find a distribution of clusters ranging from 0.5 to 6 nm, with a mean size of 2.3 nm. Therefore, the position of the Au 4f peak is indicative of the NP size only in the case of monosized clusters and cannot be directly used to estimate the NP dimensions in the presence of a broad size distribution. The valence band region, not shown here, can also be used to estimate the NP dimensions.

The valence band region of sample CAu 2 shows a decrease in the spin−orbit splitting (SOS) to about 2.30 eV (for comparison, the bulk value is 2.75 eV). The decrease in the SOS is described as an effect of quantization leading to orbital

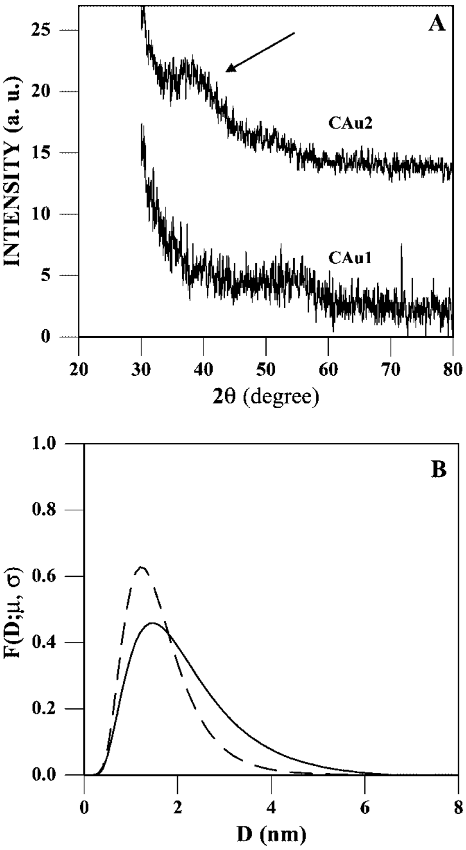

Figure 5. (A) X-ray diffraction pattern of CAu 1 and CAu 2 samples. The arrow indicates the Au diffraction peaks. (B) Size distribution function obtained from the iterative process described in the text (solid line) and the size distribution obtained from the XRD pattern of sample CAu 2 (dotted lines).

mixing.[27] Using SOS experimental data by Dicenzo and Mason, we can estimate, for sample CAu 2, a mean particle size of 2.3 nm, differing from the value obtained from the analysis of just the core line shift. Again, this effect is due to the distortion of the core line due to the size distribution spanning over a wide range of NP sizes. Both the core line position and the VB splitting represent a cumulative result of the different extent of quantum confinements in the NP distribution. The average particle sizes corresponding to the two samples are 1.65 and 2.29 nm for the two samples CAu 1 (8.24% Au) and CAu 2 (12.55% Au), respectively. These results are in agreement with those obtained by Gampp et al. concerning plasma-assisted chemical vapor deposition of a-C:H/Au.[28] These authors, in fact, measured a mean NP size of ~ 2 nm by TEM for a sample containing 11.5% of gold.

XRD Analysis. In order to check the validity of the proposed model, we compared our size distribution with that obtained by XRD analysis. In Figure 5A, we present the XRD spectra obtained for samples CAu 1 and CAu 2. The spectrum from CAu 1 sample does not show any spectral features assigned to crystalline gold nanoparticles; therefore, we cannot derive information about the size distribution for this sample. On the contrary, the CAu 2 spectrum shows a weak, broad peak at around $2\theta = 40°$, assigned to the Au(111) and Au(200) peaks. The pronounced broadening of the XRD peak is a clear indication of the small NP dimensions in the sample.[29,30] The XRD size distribution was obtained for Au(111) and Au(200) peaks (after their proper separation by fitting the spectrum by Pearson VII[31]) by the Winfit program,[32] performing the Fourier transform according to the Warren−Averbach method. Though the full Warren−Averbach analysis, considering strain distribution as well as size distribution, could not be performed because of the lack of multiple reflections, independent single-line analysis of peaks (111) and (200) gave an identical size distribution, thus confirming the reliability of the used procedure. One should note that X-ray diffraction loses sensitivity at particle sizes of about 2 nm; therefore, errors in the extracted size distribution could be rather high in this size range. Still, the resulting normalized size distribution for sample CAu 2 is presented in Figure 5B (dashed line) together with that calculated by our XPS method (continuous line). Despite the difference between the two distributions, they agree at a qualitative level in the central part. The ranges of dimensions in the two distributions are similar, the XPS one showing a stronger tail toward high dimensions, which could be associated with the Ostwald ripening of nanoclusters just on the surface after the deposition process has been stopped. One should note that the sampling depths of the two techniques are different, about 5−7 nm for XPS and the whole film thickness for XRD; therefore, if a significant difference in size distribution exists between the surface region and the bulk, different results are expected from the two techniques. The limited sampling depth of XPS is an advantage for all of those samples whose properties are especially influenced by the surface, as for heterogeneous catalysis or electrochemical gas sensors. Moreover, XPS is more sensitive with respect to XRD in the case of low Au concentrations, as was found for sample CAu 1. This is an additional advantage because it allows one to analyze thin catalyst films with small metal content, which are desirable because of the lower consumption of precious metals like Au, Pt, and Ir.

Conclusions

In this work, we have demonstrated that the size distribution of gold NPs in plasma-deposited a-C/Au samples can be derived by line shape analysis of the Au 4f photoemission spectrum. The technique works well in the analysis of NPs with sizes lower than 5 nm. Because the effects of quantum confinement increase with decreasing NP size, XPS is particularly suitable for the characterization of very small NP dimensions (<1.5 nm). This is of great interest because other analytical techniques, such as XRD and TEM, lose their sensitivity in this region. Finally, the high surface sensitivity of XPS is of particular interests for catalysis, where the characteristics of nanoparticles supported on the material surface strongly influence the properties of the catalyst.

Acknowledgment. This work was supported by NATO through Collaborative Linkage Grant PDD(CP)-(CBP.NR.CLG 982775). The authors are indebted to A. Roat for significant discussions.

References and Notes

(1) Slater, J. C.; Johnson, K. H. *Phys. Today* **1974**, *27*, 34.
(2) Moriarty, P. *Rep. Prog. Phys.* **2001**, *64*, 297.
(3) Lu, Y.; Liu, G. L.; Lee, L. P. *Nano Lett.* **2005**, *5*, 5.
(4) Baranov, A.; Fanchenko, S.; Calliari, L.; Speranza, G.; Minati, L.; Shorokhov, A. V.; Fedoseenkov, D. *Diamond Relat. Mater.* **2007**, *4−7*, 1365.
(5) Wertheim, G. K.; DiCenso, S. B.; Buchanan, D. N. E. *Phys. Rev. B* **1986**, *33*, 5384.
(6) Haruta, M.; Yamada, N.; Kobayashi, T.; Ijima, S. *J. Catal.* **1989**, *115*, 301.
(7) Valden, M.; Lai, X.; Goodman, D. W. *Science* **1998**, *281*, 1647.
(8) Lee, S.; Fan, C.; Wu, T.; Anderson, S. L. *J. Am. Chem. Soc.* **2004**, *126*, 5682.
(9) Wertheim, G. K.; DiCenzo, S. B. *Phys. Rev. B* **1988**, *37*, 844.
(10) Mason, M. G. *Phys. Rev. B* **1983**, *27*, 748.

(11) Wertheim, G. K.; DiCenzo, S. B.; Youngquist, S. E. *Phys. Rev Lett.* **1983**, *51*, 2310.

(12) Lim, D. C.; Lopez-Salido, I.; Dietsche, R.; Bubek, M.; Kim, Y. D. *Surf. Sci.* **2006**, *600*, 507.

(13) Videnovich, I. R. *Surface Characterization of Amorphous Hydrogenated Carbon Thin Films Containing Nanoclusters of Nobel Metals*; 2003; http://pages.unibas.ch/diss/2003/DabsB.6479.pdf.

(14) Kohiki, S.; Ikeda, S. *Phys. Rev. B* **1986**, *34*, 3786.

(15) Videnovich, I. R. *J. Appl. Phys.* **2005**, *97*, 074308.

(16) Boyen, H.-G.; Ethirajan, A.; Kastle, G.; Weigl, F.; Ziemann, P; Schmid, G.; Garnier, M. G.; Buttner, M.; Oelhafen, P. *Phys. Rew Lett.* **2005**, *94*, 016804.

(17) DiCenso, S. B.; Berry, S. D.; Hartford, E. H., Jr. *Phys. Rev. B* **1988**, *38*, 8465.

(18) Rao, C. N. R.; Kulkarni, G. U.; Govindaraj, A.; Satishkumar, B. C.; John Thomas, P. *Pure Appl. Chem.* **2000**, *72*, 21.

(19) Venables, J. A. *Surf. Sci.* **1994**, *299–300*, 798.

(20) Thune, E.; Carpene, E.; Sauthoff, K.; Seibt, M.; Reinke, P. *J. Appl. Phys.* **2005**, *98*, 034304.

(21) Hovel, H.; Grimm, B.; Pollmann, M.; Reihl, B. *Phys. Rev. Lett.* **1998**, *81*, 4608.

(22) Jason, T.; Mangesh, C.; Bore, T.; Datye, A. K.; Davis, R. J. *J. Catal.* **2006**, *238*, 458.

(23) Briggs, D.; Grant, J. T. *Surface Analysis by Auger and X-ray Photoelectron Spectroscopy*; IM Publications: Chichester, U.K., 2003.

(24) Cheung, T. T. P.; et al. *Surf. Sci.* **1984**, *140*, 151.

(25) Boyen, H.-G.; Kästle, G.; Weigl, F.; Ziemann, P.; Oelhafen, P. *Phys. Rev. Lett.* **2001**, *27*, 276401.

(26) Tanaka, A.; Takeda, Y.; Imamura, M.; Sato, S. *Phys. Rev. B* **2003**, *68*, 195415.

(27) Lee, S. T.; Apai, G.; Mason, M. G.; Benbow, R.; Hurych, Z. *Phys. Rev. B* **1981**, *23*, 505.

(28) Gampp, R. *Deposition und Charakterisierung von Metalhaltigen, Amorphen Kohlenwasserstoffilmen zur Anwendung in Sonnenkollektoren*; VDI: Dusseldorf, Germany, 1996.

(29) Jiang, P.; Xie, S.; Yao, J.; Pang, S.; Gao, H. *J. Phys. D* **2001**, *34*, 2255.

(30) Zhang, P.; Sham, T. K. *Phys. Rev. Lett.* **2003**, *90*, 245501.

(31) Klug, H. P., Alexander, L. E. *X-Ray Diffraction Procedures*; Wiley-Interscience: New York, 1974.

(32) GeoZentrum Nordbayern. http://www.geol.uni-erlangen.de/software/winsoft.html.

JP804169Q